AGU PUBLICATIONS

Geophysical Research Letters

RESEARCH LETTER
10.1002/2017GL075526

Key Points:
- Ceres's largest crater Kerwan has unique morphology: the deep center rises concavely to a broad topographic bench interior to the rim
- The morphology can be produced by viscous relaxation of the crater in a crust which thins substantially beneath the crater floor
- The inferred high-density material beneath Kerwan would produce a positive gravity anomaly, consistent with data from NASA's Dawn mission

Supporting Information:
- Supporting Information S1

Correspondence to:
M. T. Bland,
mbland@usgs.gov

Citation:
Bland, M. T., Ermakov, A. I., Raymond, C. A., Williams, D. A., Bowling, T. J., Preusker, F., … Russell, C. T. (2018). Morphological indicators of a mascon beneath Ceres's largest crater, Kerwan. *Geophysical Research Letters*, *45*, 1297–1304. https://doi.org/10.1002/2017GL075526

Received 1 SEP 2017
Accepted 23 JAN 2018
Accepted article online 29 JAN 2018
Published online 12 FEB 2018

Morphological Indicators of a Mascon Beneath Ceres's Largest Crater, Kerwan

M. T. Bland[1], A. I. Ermakov[2], C. A. Raymond[2], D. A. Williams[3], T. J. Bowling[4], F. Preusker[5], R. S. Park[2], S. Marchi[6], J. C. Castillo-Rogez[2], R. R. Fu[7], and C. T. Russell[8]

[1]Astrogeology Science Center, U. S. Geological Survey, Flagstaff, AZ, USA, [2]Jet Propulsion Laboratory, California Institute of Technology, Pasadena, CA, USA, [3]School of Earth and Space Exploration, Arizona State University, Tempe, AZ, USA, [4]Department of the Geophysical Sciences, University of Chicago, Chicago, IL, USA, [5]German Aerospace Center (DLR), Berlin, Germany, [6]Southwest Research Institute, Boulder, CO, USA, [7]Department of Earth and Planetary Science, Harvard University, Cambridge, MA, USA, [8]Department of Earth, Planetary, and Space Sciences, University of California, Los Angeles, CA, USA

Abstract Gravity data of Ceres returned by the National Aeronautics and Space Administration's Dawn spacecraft is consistent with a lower density crust of variable thickness overlying a higher density mantle. Crustal thickness variations can affect the long-term, postimpact modification of impact craters on Ceres. Here we show that the unusual morphology of the 280 km diameter crater Kerwan may result from viscous relaxation in an outer layer that thins substantially beneath the crater floor. We propose that such a structure is consistent with either impact-induced uplift of the high-density mantle beneath the crater or from volatile loss during the impact event. In either case, the subsurface structure inferred from the crater morphology is superisostatic, and the mass excess would result in a positive Bouguer anomaly beneath the crater, consistent with the highest-degree gravity data from Dawn. Ceres joins the Moon, Mars, and Mercury in having basin-associated gravity anomalies, although their origin may differ substantially.

1. Introduction

The National Aeronautics and Space Administration's (NASA) Dawn mission (Russell & Raymond, 2011) has been orbiting Ceres since March of 2015. The long duration of the investigation, and the relatively low orbit achieved, enabled acquisition of a high-resolution shape model and determination of gravity harmonics to degree 14 globally and 18 locally (Ermakov et al., 2017; Konopliv et al., 2017). The gravity is consistent with a two-layer internal structure consisting of a lower density "crust" (~1,287 kg m^{-3}) with an average thickness of ~40 km and a higher density (2,434 kg m^{-3}) "mantle" (Ermakov et al., 2017; Park et al., 2016). Detailed admittance analysis of the gravity (degree 3–16) and shape indicates that the thickness of the crust is laterally variable (Ermakov et al., 2017). Much (although not all) of the crustal thickness variations are associated with Ceres's largest impact craters.

The surface of Ceres is heavily cratered (Hiesinger et al., 2016; Marchi et al., 2016). Contrary to expectations (e.g., Bland, 2013), most of these craters show little evidence of viscous relaxation, in which stresses resulting from uncompensated crater topography induce viscous flow that removes the topography. Instead, most of Ceres's largest craters have apparent depths (d_a, i.e., depths relative to the surrounding terrain) greater than 2 km, with some exceeding 5 km (Bland et al., 2016). The existence of these deep craters places strong constraints on the rheology of Ceres's outer layer and indicates that the near surface cannot contain more than ~35% water ice by volume. Water ice volumes exceeding 35% would result in a rheology too weak to preserve crater topography (Bland et al., 2016; Fu et al., 2017). The inferred ice volume limit is consistent with modeling of the global relaxation of Ceres (Fu et al., 2017) and with results from Dawn's Gamma Ray and Neutron Detector instrument, which has detected 10 wt % water ice (~20% by volume) in the regolith at latitudes >45° (Prettyman et al., 2017). A pure ice/silicate composition for Ceres's outer layer is inconsistent with the density structure inferred from Dawn gravity data (Ermakov et al., 2017; Konopliv et al., 2017; Park et al., 2016), so the remaining ~65% must consist of some combination of silicates, salts, and clathrate hydrates.

Despite the existence of deep craters on Ceres, limited viscous relaxation may have occurred. Analysis of the size-frequency distribution of Ceres's craters indicates a significant dearth of craters >100 km in diameter,

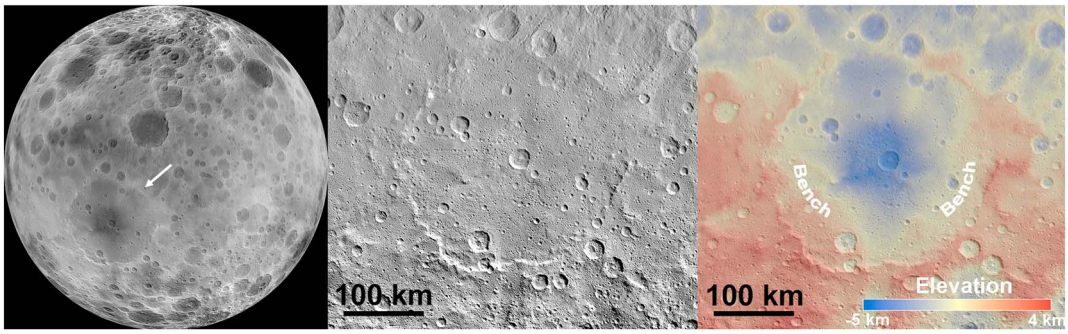

Figure 1. Kerwan as observed by NASA's Dawn spacecraft. (left) Topography data overlain on a Dawn Framing Camera (FC) mosaic in orthographic projection (centered 0°N, 150°E). Total relief shown is ~14 km. Kerwan is indicated by the white arrow. Dark regions are low, and light regions are high. (middle) A single Dawn FC clear filter image of Kerwan. Image scale is 138 m/pixel. (right) Color-coded topography relative to the best fit ellipsoid (482 km by 446 km) overlain on a Dawn FC image. Note the topographic bench interior to the crater rim and the deep center (see supporting information and Figure 2 for topographic profiles).

suggesting that the largest craters might have been removed by viscous relaxation (Marchi et al., 2016). Bland et al. (2016) also identified two craters that may exhibit evidence of viscous relaxation: the crater Coniraya, which is much shallower (d_a = 500 m) than a similar-sized, adjacent crater (Vinotonus, d_a = 5 km), and Ceres's largest crater, Kerwan (diameter D = 280 km), which has unusual topography. Local heterogeneities in surface and crater properties are common on Ceres and suggest substantial subsurface spatial heterogeneity (Raymond et al., 2017).

2. The Morphology of the Crater Kerwan

Although quite deep at its center (~5.5 km relative to the surrounding terrain), Kerwan has a peculiar morphology that deviates strongly from the steep-walled, flat-floored shape typical of complex craters, or the peak ring structures typical of large basins on terrestrial planets (Figure 1 and the supporting information; Preusker et al., 2016; Raymond et al., 2011). A pronounced topographic bench sits interior to its rim. In many places, especially on the eastern side of the crater, this bench is at, or just below, the elevation of the terrain outside the crater (see average topographic profile in Figures 2 and S1). Thus, despite its maximum depth, much of the floor sits just 1–2 km lower than the surrounding terrain. The bench is less pronounced in the northern portion of the crater. The surface of the topographic bench varies from relatively flat to gently sloping toward the crater center. The slope of the bench/floor increases toward the crater center, resulting in a concave-down shape (Figure 2). The central portion of the crater floor (within ~45 km of the center) is deep, relatively flat, and pierced by a 26 km diameter crater (Insitor). No central structure (peak or peak ring) is observed. The topography of Kerwan contrasts with that of other large craters on Ceres, which, with the exception of Yalode (see below and Crown et al., 2017), have a more classic complex crater morphology (see supporting information in Bland et al., 2016).

Kerwan is the oldest confirmed crater on Ceres, as evidenced by its highly degraded rim, lack of ejecta blanket, and heavily cratered interior (Williams et al., 2017). The crater is situated in a region of smooth terrain which covers both the crater exterior and interior (Hiesinger et al., 2016; Williams et al., 2017). The origin of the smooth terrain remains unclear, but its existence within the crater suggests it is not impact ejecta from Kerwan. There is also no unambiguous evidence for (cryo)volcanism having modified Kerwan itself (Hiesinger et al., 2016, Williams et al., 2017). Instead, the smooth terrain may be impact melt resulting from the Kerwan impact (Williams et al., 2017, and see discussion below).

We hypothesize that Kerwan's unique morphology results from viscous relaxation. The rate at which a crater will viscously relax depends both on its size and the viscosity (i.e., temperature and material) of the substrate. Given its size, age, and location (centered at 10°S latitude, a surface temperature of 155 K; e.g., Hayne & Aharonson, 2015; Schorghofer, 2016), Kerwan is the crater most likely to have undergone viscous relaxation on Ceres. To test this hypothesis, we performed a suite of numerical simulations to assess whether Kerwan's distinctive shape can be reproduced by viscous relaxation.

3. Simulating Viscous Relaxation of Kerwan

We simulate viscous relaxation of the Kerwan impact crater using the finite element model Tekton v2.3 (Melosh & Raefsky, 1980) in axisymmetric geometry. Our approach follows the methodology described in Bland et al. (2016) and Bland (2013). The model imposes a flat-floored crater on the surface of the simulation domain and allows the initial topography and the stress it induces to relax by viscoelastic deformation under the influence of gravity. We assume an initial crater shape that is 140 km in radius (280 km in diameter) and 5.5 km deep relative to the surrounding terrain. The floor of the crater is flat until a radius of 85 km, at which point the rim wall rises rapidly (modeled as a second-order polynomial) to the rim, which stands 1 km above the surrounding terrain. This classic "pie-tin" shape is consistent with other large, fresh craters on Ceres (Hiesinger et al., 2016), including the 170 km diameter crater Urvara and the 140 km diameter crater Vinotonus (see Bland et al., 2016, for topography of Ceres's largest craters), and provides a simple initial shape to which subsequent deformation can be compared. In reality, Kerwan's postimpact shape was plausibly more similar to that of Yalode (D = 260 km), which has a peak ring-like morphology (Figure S4). However, we find that our basic conclusions are independent of whether a flat-floor or Yalode-like initial shape is used (see supporting information and Figure S5). Our model domain is 420 km wide and up to 100 km deep, with a horizontal resolution of 1 km, and a variable vertical resolution (maximum 100 m). The bottom of the domain is fixed, the sides are free slip, and the top is a free surface (Figure 2).

Tekton v2.3 does not explicitly include thermodynamics, but the viscosity structure is determined by externally calculating the thermal structure resulting from radiogenic heating and allowing it to evolve in time. The present-day radiogenic heat flux is ~1 mW m^{-2} and was ~1.5 mW m^{-2} 1 Gyr ago. We use a surface temperature of 155 K, appropriate for the near-equatorial location of Kerwan (Hayne & Aharonson, 2015; Schorghofer, 2016).

The simulations are viscoelastic and assume that flow is accommodated by water ice with a viscosity modulated by a substantial component (>65%) of non-ice particulate material (e.g., Durham et al., 2009; Durham et al., 1992; Mangold et al., 2002). We use all known flow regimes for ice I in a combined constitutive flow law that includes diffusion and dislocation creep, grain boundary sliding, and basal slip (e.g., Durham & Stern, 2001). Diffusion and grain boundary are grain size sensitive, and we nominally use a grain size of 1 mm. We account for the effect of non-ice material by increasing the resulting effective viscosity relative to pure ice. Laboratory measurements of the deformation of rock-ice mixtures indicates that the viscosity of ice increases by ~100 times as the particulate content reaches 60% (Durham et al., 1992, et al., 2009; Friedson & Stevenson, 1983; Mangold et al., 2002). At particulate content >60–70% the material becomes "jammed" and the viscosity of the mixture increase dramatically. Bland et al. (2016) found that an effective viscosity at least 1,000 times greater than water ice is required to retain crater topography on Ceres, and we adopt their value here.

Because of the thermal gradient imposed, the viscosity of the crust is highest near the surface and decreases with depth (unless a viscosity interface is imposed), consistent with Bland et al. (2016) and Fu et al. (2017). The effective viscosity at the cold surface is ~10^{25} Pa s, and minimum viscosities at depth are ~10^{22} Pa s. The surface viscosity is identical to that inferred by Fu et al. (2017) from models of global relaxation, whereas the minimum viscosity in our model is consistent with the lower bound on the viscosity decrease with depth they infer (1 order of magnitude every 15 km). Decreasing the viscosity at depth in our model (equivalent to a modest increase in the assumed thermal gradient) while maintaining the surface viscosity at ~10^{25} only increases the rate our simulated Kerwan deforms and does not change its final morphology.

We investigate a range of subsurface structures including a uniform layer (i.e., a half-space wherein the viscosity decreases with depth), a layered structure in which an outer layer of uniform thickness overlies a less-mobile (higher viscosity) layer at depth, and a layered structure in which the outer layer includes lateral variations in thickness (e.g., thinner beneath the crater). When a "high-viscosity" layer is imposed at depth we simply increase its viscosity by 100 times relative to the material above (e.g., ~10^{25} Pa s compared to 10^{23} Pa s), which is enough to essentially completely retard viscous flow. Stresses in the model are initialized as lithostatic with a perturbation due to the crater topography (Dombard & McKinnon, 2006). We impose a gravitational acceleration of 0.27 m s^{-2}. Given the uncertainty in the age of Kerwan (Williams et al., 2017 and see supporting information) we nominally permit the topography to evolve for 1–2 Ga, consistent with the maximum age of the smooth terrain filling the crater.

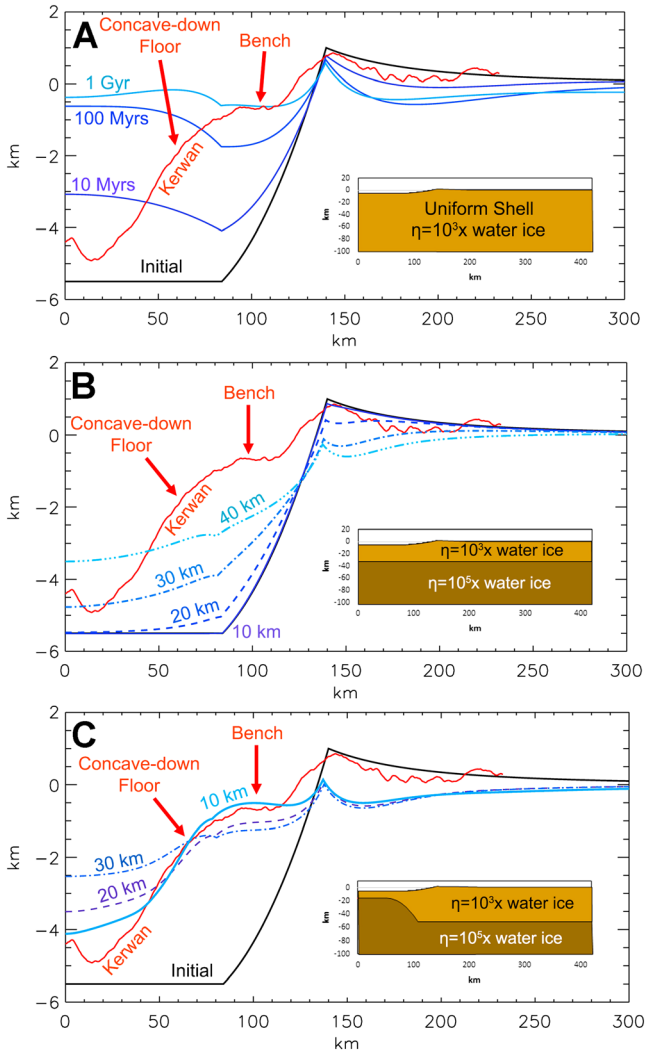

Figure 2. Comparison of Kerwan's topography (red curve) and numerical simulations of viscous relaxation (blue curves) for different subsurface structures (shown in insets). The Kerwan profile is an average of 15 radial profiles (see supporting information Text S1 and Figure S1). The location of the topographic bench and "concave-down" floor discussed in the text are indicated. Note that the topographic depression and apparent peak near the center of the average profile is due to several individual profiles transecting the small crater Insitor within Kerwan (see Figure S1). In each panel the simulated initial crater topography is shown in black. (a) A uniform rheology model. Viscosity decreases with depth due to the radiogenically driven thermal gradient, but no discontinuities are used. Each curve shows a different time step of the same simulation (violet, 10 Ma; blue, 100 Ma; and light blue, 1 Ga). (b) A model with a thin low-viscosity layer (crust) underlain by a higher-viscosity (100 times relative to the crust) layer. Each curve shows a different layer thickness. The lightest blue dash-dot-dot-dot line is for a 40 km thick layer. The blue dot-dashed line is for a 30 km thick layer. The dark blue dashed line is for a 20 km thick layer. The purplish solid line is for a 10 km thick layer (line overlaps the black profile of the initial crater). (c) A model in which the crust thins beneath the crater and thickens outside the crater. The light blue curve is our best fit simulated topography and uses a minimum crustal thickness of 10 km. The violet dashed curve and blue dot-dashed curve have a similar structure to the best fit model, but the crustal thickness beneath the crater is 20 km and 30 km, respectively.

4. Simulation Results: Inferring Nonuniform Crustal Thickness Beneath Kerwan

Our modeling results are summarized in Figure 2. The morphology of our simulated viscously relaxed Kerwan-like crater is strongly influenced by Ceres's local subsurface structure. When a rheologically uniform interior (viscosity decreases with depth due to the thermal gradient, but no abrupt viscosity transitions are imposed) is assumed (Figure 2a), the resulting crater has a classic relaxation morphology (e.g., Scott, 1967). The longest topographic wavelengths relax the fastest, resulting in upward doming of the crater floor and formation of a topographic moat interior to the crater rim. The morphology is reminiscent, though at a larger scale, of viscously relaxed craters on icy satellites (e.g., Bland et al., 2012). After 1 Gyr of relaxation, the crater center has reached the approximate elevation of the terrain outside the crater (i.e., the zero-potential surface). Short wavelengths are preserved, such that the initial crater rim is essentially unmodified. At no point in the evolution of the crater topography does the simulated morphology resemble that observed at Kerwan. We therefore conclude that Kerwan's morphology did not result from viscous relaxation in a rheologically uniform outer layer, a structure consistent with global relaxation models (Fu et al., 2017).

Dawn gravity data are consistent with a two-layer model in which a low-density crust overlies a higher-density interior (Ermakov et al., 2017; Park et al., 2016). If the density interface at depth also corresponds (at least locally) to a viscosity interface, the viscous relaxation process is fundamentally altered. Parmentier and Head (1981) showed analytically that the presence of a near-surface immobile layer at depth both retards relaxation and modifies its wavelength dependence such that long-wavelength topography is preserved and short wavelengths are removed. The effect of a high-viscosity layer at depth on viscous relaxation of Kerwan is shown in Figure 2b (see also Figure S2). We initially assume a flat interface between the outer lower-viscosity crust (in which viscous flow occurs) and the deeper higher-viscosity mantle (100 times the viscosity of the crust), which is effectively immobile.

We find that the presence of high-viscosity material at depth inhibits viscous relaxation, supporting the previous work of Parmentier and Head (1981). For a 40 km thick crust (Ermakov et al., 2017, infer an average crustal thickness of 41 km), the simulated crater retains a depth of 3.5 km after 1 Gyr: substantially deeper than when a uniform model is assumed (Figure 2a). For crustal thicknesses less than 40 km, even deeper craters are preserved, and in the case of a crust just 10 km thick, viscous relaxation becomes completely inhibited. For greater thickness, the deformation approaches that of our uniform model: a layer 70 km thick results in topography nearly identical to that of the uniform model after 1 Gyr. Kerwan's morphology is simply insensitive to crustal structure at depths greater than ~70 km. Notably, viscous relaxation in a thin layer also results in removal of the crater rim, as previously predicted (Parmentier & Head, 1981).

Viscous relaxation in a thin shell reproduces some of Kerwan's morphology. Substantial crater depth can be preserved, the crater lacks a moat interior to the rim (as occurs in the uniform rheology model), and the crater rim is reduced. Despite this, the overall simulated morphology is

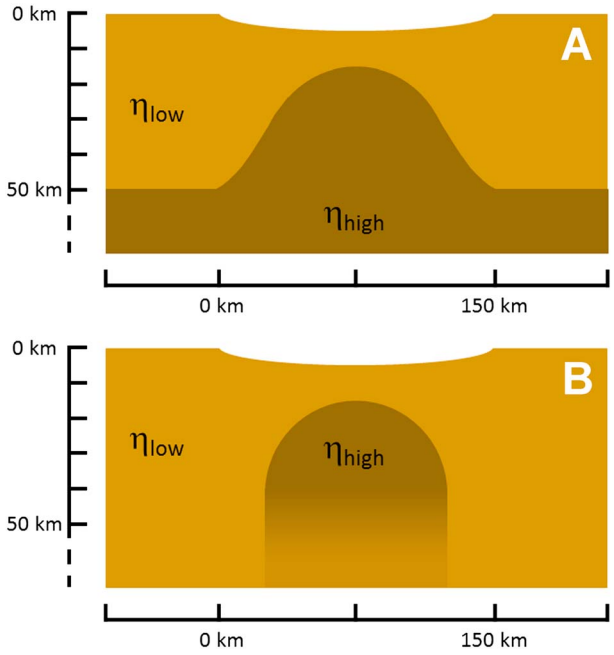

Figure 3. Two possible inferred subsurface structures beneath Kerwan. (a) Upward deflection of a high-viscosity (η) mantle beneath the crater. (b) Devolatilization of a plug of material beneath Kerwan, which increased the density and viscosity of the material. The details of the subsurface structure shown here have been selected to reproduce Kerwan's specific morphology. The latter case (b) is more consistent with other Dawn observations.

inconsistent with that observed at Kerwan. Crucially, the distinctive topographic bench interior to the crater rim is not reproduced nor is the unusual concave-down shape of the floor. Instead, the floor of the simulated crater is concave-up. We therefore conclude that Kerwan's morphology is inconsistent with viscous relaxation in a thin rheologically weak crust of uniform thickness.

Because the simplistic models described above failed to reproduce Kerwan's morphology, we explored scenarios in which the crustal thickness varies significantly within the simulation domain. Whereas a two-layer density structure with uniform layer thickness is the simplest first-order assumption for Ceres's interior structure, higher-order gravity data from Dawn indicates the thickness of the outer layer is laterally variable (Ermakov et al., 2017; Konopliv et al., 2017). Similar crustal thickness variations have been observed on the terrestrial planets. High-resolution gravity data of the Moon, for example, have revealed basin-associated deflections of the crust-mantle interface (e.g., Zuber et al., 2016). In the case of Orientale (D = 320–460 km), the mantle beneath the impact crater is uplifted by nearly 35 km, reducing the crustal thickness from ~45 km to just ~10 km beneath the crater (Zuber et al., 2016). Although smaller than Orientale and forming under different gravitational, thermal, and material conditions, the Kerwan-forming impact may have produced a qualitatively similar deflection of the inner-outer layer density boundary.

To evaluate the effects of a nonuniform outer layer thickness on crater relaxation, we performed a suite of simulations that investigated a broad range of crust-mantle interface geometries. The topography from our best fit simulation is shown in Figure 2c, along with that resulting from several alternative interior structures (also see Figure S3). The best fit simulation assumed a 10 km thick crust beneath the crater floor. The thin crust beneath the crater center persists over one third of the crater radius (i.e., to a radius of 50 km from the crater center). The thickness increases rapidly beyond that radius, reaching a maximum thickness of 50 km at 110 km from the crater center (inset of Figure 2c). The structure is, perhaps coincidently, analogous to that inferred beneath Orientale on the Moon (Zuber et al., 2016). As in the uniform thickness case, the deeper layer has an effective viscosity 100 times greater than the crust. Assuming this structure, viscous relaxation over 1 Gyr successfully reproduces most of Kerwan's distinctive morphology. The thin crust beneath the center of the crater prevents viscous flow, preserving the deep topography at Kerwan's center. Flow can occur in the thicker portion of the layer, and long wavelengths viscously relax in the outer two thirds of the crater to produce the topographic bench interior to the crater rim and the concave-down topography. Because even the maximum thickness is restricted relative to the uniform model, the rim amplitude is also decreased. The rim amplitude is smaller than that in the average Kerwan profile (similar to the thin-crust simulation in Figure 2b), although individual profiles do show a muted rim in some cases.

The resulting crater topography depends sensitively on the geometry of the subsurface structure, which must be tuned to reproduce the observed location and amplitude of the interior bench (supporting information and Figure S3). Increasing the thickness of the crust beneath the crater center to 20 or 30 km (while maintaining a 50 km crust exterior to the crater) allows increased flow in the wider channel, resulting in reduced simulated crater depth and a less-pronounced topographic bench interior to the rim. The lateral extent of the thinned portion of the crust is also constrained. If the thinned region extends farther from the crater center, flow is inhibited beneath the outer portion of the crater and the topographic bench does not form (Figure S3). In contrast, if the thinned region is smaller in extent, Kerwan's flat floor is not reproduced. In short, Kerwan's observed surface morphology can directly constrain the detailed subsurface structure beneath the crater (see supporting information).

5. The Origin of Kerwan's Subsurface Structure and Gravity Anomaly

The local subsurface structure inferred from Kerwan's morphology can result from at least two different mechanisms (Figure 3), possibly in combination. One end-member is that the Kerwan-forming impact resulted in uplift of the crust-mantle boundary (Figure 3a), as frequently occurs during impacts on the terrestrial planets (e.g., Dombard et al., 2013; Neumann et al., 1996, 2004; Wieczorek & Phillips, 1999). This hypothesis implicitly assumes that the density contrast revealed by gravity data (Ermakov et al., 2017; Park et al., 2016) also corresponds to a viscosity contrast: higher densities might imply a greater silicate component and thus increased viscosity. Models of the relaxation of Ceres's global topography indicate, however, that despite the inferred density transition, there is no corresponding viscosity increase within the upper 100 km of the surface at global scales (Fu et al., 2017). The higher-density mantle must therefore have a viscosity similar to (or less than) the crust directly above it, implying a fluid saturated, potentially soft sediment-like composition (Fu et al., 2017). At least at global scales, Ceres's mantle therefore appears to be quite weak ($\leq 10^{21}$ Pa s). Whereas the uplifted structure we infer has precedent on the terrestrial planets, it requires that the local mantle beneath Kerwan is rheologically distinct from the global average.

An alternative endmember is that the temperature perturbation induced by the Kerwan-forming impact resulted in local volatile loss beneath the crater (Figure 3b). Simulations of large impacts (resulting in craters with $D = 180$ km) into mixed ice-rock targets on Mars (a reasonable analog for Ceres's ice-rock-salt-clathrate composition) result in widespread melting of interstitial ice to depths of several tens of kilometers (Ivanov & Pierazzo, 2011), although the impact velocity used, which controls peak temperature, was modestly higher than typical values on Ceres (8 km/s in Ivanov & Pierazzo, 2011, versus ~5 km/s in the asteroid belt, Bottke et al., 1994). Marchi et al. (2013) further showed that a 10 km projectile hitting Vesta at 5–7 km s^{-1} can result in subsurface temperature increases of several hundred kelvin. Given surface temperatures of ~155 K at Kerwan (and even warmer subsurface temperatures), a local temperature increase of 100–200 K is sufficient to cause melting. Further, Bowling et al. (2016) showed that subsurface temperatures can exceed 300 K for the much smaller Occator-forming impact ($D = 90$ km). These simulations suggest that a Kerwan-sized impact on Ceres would result in melting or perhaps even vaporization of the ~30% water ice in the subsurface beneath the crater, and of clathrate hydrates. Temperatures may also be sufficient for substantial water loss from hydrated salts such as hydrohalite (Castillo-Rogez et al., 2017) and clays (Gavin & Chevrier, 2010). The residual plug of devolatilized material beneath the crater would be modestly higher in both viscosity (only a 100 times increase is required) and density relative to the preexisting crust. The devolatilized region is likely to begin in the shallow subsurface where peak impact temperatures are reached, modestly higher than our best fit model. High-viscosity material in the immediate subsurface would prevent any relaxation of the crater center; however, this is consistent with our simulations if a shallower initial crater is used. Based on our deep initial crater shape, we only require that the zone of high-viscosity material must begin within 10 km of the surface and extend tens of kilometers in depth. In this hypothesis, the mantle (whether weak or strong) has no effect on the relaxation. The high-viscosity plug simply results from an impact-induced compositional change in the crust beneath Kerwan.

The water liberated in such an impact would percolate upward, potentially dissolving highly soluble material, such as salts, and transporting them to the surface. Data from Dawn's Visible and Infrared Spectrometer instrument indicates that the Kerwan region (along with regions surrounding Inamahari and Dantu craters to the north) has a higher albedo relative to "average" Ceres, and relatively deep absorptions at 3.1 μm due to ammoniated clays (Ammannito et al., 2016). The deposition of salts, including ammoniated species (De Sanctis et al., 2016), would brighten the surface locally, consistent with the Visible and Infrared Spectrometer observations. Temperatures sufficient for liquid water percolation might also result in transport (or loss) of ammonium. Notably, the 3.1 μm absorption enhancement has also been correlated with a putative ancient basin (Vendimia Planitia), suggesting that impact induced excavation and/or alteration has also occurred elsewhere on Ceres (Marchi et al., 2016). Such enhancements are not observed at Yalode (similar in size to Kerwan), suggesting Ceres's subsurface is spatially heterogeneous (Raymond et al., 2017) or that the impact speeds were quite different. The Kerwan region and the smooth terrain associated with it also have a dearth of surface features characteristic of ground ice relative to similar latitudes on Ceres (Schmidt et al., 2017; Sizemore et al., 2017; Williams et al., 2017), and pitted terrain, which is thought to form by volatile loss, is not observed in the region (at least at image scales of 35 m/pixel) (Sizemore et al., 2017). These observations may indicate that the region is now volatile poor, perhaps due to extensive volatile loss during emplacement of the impact-generated smooth terrain.

In reality, both mantle uplift and devolatilization likely occurred during the Kerwan-forming impact, and for both end-members we predict high-density material in the near subsurface beneath Kerwan. These high-density regions would be expected to produce a positive mass anomaly within the basin. Superisostatic mantle uplift beneath basins have been hypothesized to be the cause of lunar "mascons" (Neumann et al., 1996; Wieczorek & Phillips, 1999), although it is now recognized that such uplifts may be difficult to maintain against relaxation in the hot, postimpact lunar mantle (Pierazzo & Melosh, 2000). Instead, lunar mascons probably result from thickening of a collar of crustal material nearer the crater rim and isostatic adjustment of an expansive melt sheet (Melosh et al., 2013). If the structure we infer beneath Kerwan is the result of uplifted mantle material, the high crust/mantle density contrast on Ceres would result in an extremely large residual gravity anomaly of ~1,200 mGal (supporting information). In contrast, devolatilization would result in a much smaller density contrast, and thus a smaller residual gravity anomaly. If the original crust (density 1,287 kg m^{-3}) contained 30% water ice and/or clathrate and all the water was lost during the impact, the density of the remaining material would be just ~1,450 kg m^{-3}. Such a density contrast would result in a residual anomaly of just ~100 mGal (supporting information). The unknown porosity of the crust (e.g., Fu et al., 2017), and porosity evolution during the impact event, adds uncertainty to this estimate, but it is roughly consistent with observations. Analysis of the highest-degree gravity data available from Dawn indicates a positive Bouguer anomaly beneath Kerwan with amplitudes of 110 mGal and a positive isostatic anomaly of 20 mGal (a similar-sized anomaly is also observed at the large crater Yalode; see supporting information) (Ermakov et al., 2017; Konopliv et al., 2017). The gravity data and the global constraints on the mantle rheology both therefore favor the devolatilization hypothesis. Thus, Ceres joins the Moon (e.g., Muller & Sjogren, 1968), Mars (Smith et al., 1993), and Mercury (Smith et al., 2012) in having basin-associated gravity anomalies; however, Ceres's "mascons" may originate from impact-induced processing of its compositionally complex crust, a mechanism quite distinct from those forming mascons on the terrestrial planets.

Acknowledgments
This work was supported by NASA's Dawn at Ceres Guest Investigator Program (NNH15AZ85I). Special thanks to the Dawn mission operations team who have gone above and beyond to return exceptional data from Ceres. Jay Melosh and an anonymous reviewer provided insightful comments that improved this manuscript. All data used in this analysis are available through NASA's Planetary Data System (PDS).

References

Ammannito, E., De Sanctis, M. C., Ciarniello, M., Frigeri, A., Carrozzo, F. G., Combe, J.-P., et al. (2016). Distribution of phyllosilicates on the surface of Ceres. *Science*, *353*(6303), aaf4279. https://doi.org/10.1126/science.aaf4279

Bland, M. T. (2013). Predicted crater morphologies on Ceres: Probing internal structure and evolution. *Icarus*, *226*(1), 510–521. https://doi.org/10.1016/j.icarus.2013.05.037

Bland, M. T., Raymond, C. A., Schenk, P. M., Fu, R. R., Kneissl, T., Pasckert, J. H., et al. (2016). Composition and structure of the shallow subsurface of Ceres revealed by crater morphology. *Nature Geoscience*, *9*(7), 538–542. https://doi.org/10.1038/ngeo2743

Bland, M. T., Singer, K. N., McKinnon, W. B., & Schenk, P. M. (2012). Enceladus' extreme heat flux as revealed by its relaxed craters. *Geophysical Research Letters*, *39*, L17204. https://doi.org/10.1029/2012GL052736

Bottke, W. F., Nolan, M. C., Greenberg, R., & Kolvoord, R. A. (1994). Velocity distributions among colliding asteroids. *Icarus*, *107*(2), 255–268. https://doi.org/10.1006/icar.1994.1021

Bowling, T. J., Ciesla, F. J., Marchi, S., Johnson, B. C., Davison, T. M., Castillo-Rogez, J. C., et al. (2016). Impact induced heating of Occator crater on asteroid 1 Ceres. Presented at the 47th Lunar and Planetary Science Conference, Houston TX.

Castillo-Rogez, J. C., Young, E. D., Neveu, M., Raymond, C. A., Rivkin, A. S., Prettyman, T. H., … Russell, C. T. (2017). Ceres' astrobiological significance: Pre- and post-Dawn perspectives, #3594. Presented at the Astrobiology Science Conference, Mesa AZ.

Crown, D. A., Sizemore, H. G., Yingst, R. A., Mest, S. C., Platz, T., Berman, D. C., et al. (2017). Geologic mapping of the Urvara and Yalode Quadrangles of Ceres. *Icarus*. in press. https://doi.org/10.1016/j.icarus.2017.08.004

De Sanctis, M. C., Raponi, A., Ammannito, E., Ciarniello, M., Toplis, M. J., McSween, H. Y., et al. (2016). Bright carbonate deposits as evidence of aqueous alteration on (1) Ceres. *Nature*, *536*(7614), 54–57. https://doi.org/10.1038/nature18290

Dombard, A. J., Hauck, S. A., & Balcerski, J. A. (2013). On the origin of mascon basins on the Moon (and beyond). *Geophysical Research Letters*, *40*, 28–32. https://doi.org/10.1029/2012GL054310

Dombard, A. J., & McKinnon, W. B. (2006). Elastoviscoplastic relaxation of impact crater topography with application to Ganymede and Callisto. *Journal of Geophysical Research*, *111*, E01001. https://doi.org/10.1029/2005JE002445

Durham, W. B., Kirby, S. H., & Stern, L. A. (1992). Effects of dispersed particulated on the rheology of water ice at planetary conditions. *Journal of Geophysical Research*, *97*(E12), 20,883–20,897. https://doi.org/10.1029/92JE02326

Durham, W. B., Pathare, A. V., Stern, L. A., & Lenferink, H. J. (2009). Mobility of icy sand packs, with application to Martian permafrost. *Geophysical Research Letters*, *36*, L23203. https://doi.org/10.1029/2009GL040392

Durham, W. B., & Stern, L. A. (2001). Rheological properties of water ice—Applications to satellites of the outer planets. *Annual Review of Earth and Planetary Sciences*, *29*(1), 295–330. https://doi.org/10.1146/annurev.earth.29.1.295

Ermakov, A. I., Fu, R. R., Castillo-Rogez, J. C., Raymond, C. A., Park, R. S., Preusker, F., et al. (2017). Constraints on Ceres' internal structure and evolution from its shape and gravity measured by the Dawn spacecraft. *Journal of Geophysical Research*, *122*, 1–27. https://doi.org/10.1002/2017JE005302

Friedson, A. J., & Stevenson, D. J. (1983). Viscosity of rock-ice mixtures and applications to the evolution of the icy satellites. *Icarus*, *56*(1), 1–14. https://doi.org/10.1016/0019-1035(83)90124-0

Fu, R. R., Ermakov, A. I., Marchi, S., Castillo-Rogez, J. C., Raymond, C. A., Hager, B. H., et al. (2017). The interior structure of Ceres as revealed by surface topography. *Earth and Planetary Science Letters*, *476*, 153–164. https://doi.org/10.1016/j.epsl.2017.07.053

Gavin, P., & Chevrier, V. (2010). Thermal alteration of nontronite and montmorillonite: Implications for the Martian surface. *Icarus*, *208*(2), 721–734. https://doi.org/10.1016/j.icarus.2010.02.027

Hayne, P. O., & Aharonson, O. (2015). Thermal stability of ice on Ceres with rough topography. *Journal of Geophysical Research*, *120*, 1567–1584. https://doi.org/10.1002/2015JE004887

Hiesinger, H., Marchi, S., Schmedemann, N., Schenk, P., Pasckert, J. H., & Neeseman, A., … Raymond, C. A. (2016). Cratering on Ceres: Implications for its crust and evolution. *Science*, *353*. aaf4758. https://doi.org/10.1126/science.aaf4759

Ivanov, B. A., & Pierazzo, E. (2011). Impact cratering in H_2O-bearing targets on Mars: Thermal field under craters as starting conditions for hydrothermal activity. *Meteoritics and Planetary Science*, *46*(4), 601–619. https://doi.org/10.1111/j.1945-5100.2011.01177.x

Konopliv, A. S., Park, R. S., Vaughan, G., Bills, B. G., Asmar, S. W., Ermakov, A. I., et al. (2017). The Ceres gravity field, spin pole, rotation period and orbit from the Dawn radiometric tracking and optical data. *Icarus*, *299*, 411–429. https://doi.org/10.1016/j.icarus.2017.08.005

Mangold, N., Allemand, P., Duval, P., Geraud, Y., & Thomas, P. (2002). Experimental and theoretical deformation of ice-rock mixtures: Implications on rheology and ice content of Martian permafrost. *Planetary and Space Science*, *50*(4), 385–401. https://doi.org/10.1016/S0032-0633(02)00005-3

Marchi, S., Bottke, W. F., Cohen, B. A., Wunnemann, K., Kring, D. A., McSween, H. Y., et al. (2013). High-velocity collisions from the lunar cataclysm recorded in asteroidal meteorites. *Nature Geoscience*, *6*, 303–307. https://doi.org/10.1038/ngeo1769

Marchi, S., Ermakov, A. I., Raymond, C. A., Fu, R. R., O'Brien, D. P., Bland, M. T., et al. (2016). The missing large impact craters on Ceres. *Nature Communications*, *7*, 12,257. https://doi.org/10.1038/ncomms12257

Melosh, H. J., Freed, A. M., Johnson, B. C., Blair, D. M., Andrews-Hanna, J. C., Neumann, G. A., et al. (2013). The origin of lunar mascon basins. *Science*, *340*(6140), 1552–1555. https://doi.org/10.1126/science.1235768

Melosh, H. J., & Raefsky, A. (1980). The dynamical origin of subduction zone topography. *Geophysical Journal of the Royal Astronomical Society*, *60*(3), 333–354. https://doi.org/10.1111/j.1365-246X.1980.tb04812.x

Muller, P. M., & Sjogren, W. L. (1968). Mascons: Lunar mass concentrations. *Science*, *161*(3842), 680–684. https://doi.org/10.1126/science.161.3842.680

Neumann, G. A., Zuber, M. T., Smith, D. E., & Lemoine, F. G. (1996). The lunar crust: Global structure and signature of major basins. *Journal of Geophysical Research*, *101*(E7), 16,841–16,863. https://doi.org/10.1029/96JE01246

Neumann, G. A., Zuber, M. T., Wieczoreck, M. A., McGovern, P. J., Lemoine, F. G., & Smith, D. E. (2004). Crustal structure of Mars from gravity and topography. *Journal of Geophysical Research*, *109*, E08002. https://doi.org/10.1029/2004JE002262

Park, R. S., Konopliv, A. S., Bills, B. G., Rambauz, N., Castillo-Rogez, J. C., Raymond, C. A., et al. (2016). A partially differentiated interior for (1) Ceres deduced from its gravity field and shape. *Nature*, *537*(7621), 515–517. https://doi.org/10.1038/nature18955

Parmentier, E. M., & Head, J. W. (1981). Viscous relaxation of impact craters on icy planetary surfaces: Determination of viscosity variation with depth. *Icarus*, *47*(1), 100–111. https://doi.org/10.1016/0019-1035(81)90095-6

Pierazzo, E., & Melosh, H. J. (2000). Melt production in oblique impacts. *Icarus*, *145*(1), 252–261. https://doi.org/10.1006/icar.1999.6332

Prettyman, T. H., Yamashita, N., Toplis, M. J., McSween, H. Y., Schorghofer, N., & Marchi, S. (2017). Extensive water ice within Ceres' aqueously altered regolith: Evidence from nuclear spectroscopy. *Science*, *355*(6320), 55–59. https://doi.org/10.1126/science.aah6765

Preusker, F., Scholten, F., Matz, K.-D., Elgner, S., Jaumann, R., Roatsch, T., Joy, S. P., … Russell, C. T. (2016). Dawn at Ceres—Shape model and rotation state. Presented at the 47th Lunar and Planetary Science Conference, Houston, TX.

Raymond, C. A., Ermakov, A. I., Park, R. S., Marchi, S., Bland, M. T., Fu, R. R., … Russell, C. T. (2017). Large-scale heterogeneity of Ceres: Clues to interior evolution, #1506. Present at the 48th Lunar and Planetary Science Conference, Houston TX.

Raymond, C. A., Jaumann, R., Nathues, A., Sierks, H., Roatsch, T., Preusker, F., et al. (2011). The Dawn topography investigation. *Space Science Reviews*, *163*(1-4), 487–510. https://doi.org/10.1007/s11214-011-9863-z

Russell, C. T., & Raymond, C. A. (2011). The Dawn mission to Vesta and Ceres. *Space Science Reviews*, *163*(1-4), 3–23. https://doi.org/10.1007/s11214-011-9836-2

Schmidt, B. E., Hughson, K. H., Chilton, H. T., Scully, J. E. C., Platz, T., Nathues, A., et al. (2017). Geomorphological evidence for ground ice on dwarf planet Ceres. *Nature Geoscience*, *10*(5), 338–343. https://doi.org/10.1038/ngeo2936

Schorghofer, N. (2016). Predictions of depth-to-ice on asteroids based on an asynchronous model of temperature, impact stirring, and ice loss. *Icarus*, *276*, 88–95. https://doi.org/10.1016/j.icarus.2016.04.037

Scott, R. F. (1967). Viscous flow of craters. *Icarus*, *7*(1-3), 139–148. https://doi.org/10.1016/0019-1035(67)90058-9

Sizemore, H. G., Platz, T., Schorghofer, N., Prettyman, T. H., De Sanctis, M. C., Crown, D. A., et al. (2017). Pitted terrains on (1) Ceres and implications for shallow subsurface volatile distribution. *Geophysical Research Letters*, *44*, 6570–6578. https://doi.org/10.1002/2017GL073970

Smith, D. E., Lerch, F. J., Nerem, R. S., Zuber, M. T., Patel, G. B., Fricke, S. K., & Lemoine, F. G. (1993). An improved gravity model for Mars: Goddard Mars model 1. *Journal of Geophysical Research*, *98*(E11), 20,871–20,889. https://doi.org/10.1029/93JE01839

Smith, D. E., Zuber, M. T., Phillips, R. J., Solomon, S. C., Hauck, S. A., Lemione, F. G., et al. (2012). Gravity field and internal structure of Mercury from MESSENGER. *Science*, *336*(6078), 214–217. https://doi.org/10.1126/science.1218809

Wieczorek, M. A., & Phillips, R. J. (1999). Lunar multiring basins and the cratering process. *Icarus*, *139*(2), 246–259. https://doi.org/10.1006/icar.1999.6102

Williams, D. A., Kneissl, T., Neesemann, A., Mest, S. C., Palomba, E., Platz, T., et al. (2017). The geology of the Kerwan quadrangle of dwarf planet Ceres: Investigating Ceres' oldest, largest impact basin. *Icarus*. in press. https://doi.org/10.1016/j.icarus.2017.08.015

Zuber, M. T., Smith, D. E., Neumann, G. A., Goossens, S., Andrews-Hanna, J. C., Head, J. W., et al. (2016). The gravity field of the Orientale basin from the Gravity Recovery and Interior Laboratory mission. *Science*, *354*(6311), 438–441. https://doi.org/10.1126/science.aag0519